JACS Au
AN OPEN ACCESS JOURNAL OF THE AMERICAN CHEMICAL SOCIETY

pubs.acs.org/jacsau
Article

Direct Edge Functionalization of Corannulene−Coronene Hybrid Nanographenes

Jovana Stanojkovic, Natalia Terenti, and Mihaiela C. Stuparu*

Cite This: JACS Au 2025, 5, 1707−1716
Read Online

ABSTRACT: For more than a century, electrophilic aromatic substitution reactions have been central to the construction of a rich variety of organic molecules that are useful in all aspects of human life. Typically, small aromatic nuclei, such as benzene, provide an ideal substrate. An increase in the number of annulated aromatic rings enhances the number of potential reactive sites and frequently results in complex product mixtures. Thus, nanographenes with a relatively large aromatic system are seldom selective in their substitution positions. Moreover, nanographene substrates with a scope for multiple substitution reactions and patterns remain rare. Herein, we demonstrate that a curved aromatic system based on a corannulene−coronene hybrid structure comprising 48 conjugated sp^2-carbon atoms allows for direct and regioselective edge functionalization through bromination, nitration, formylation, and Friedel−Crafts acylation in good yields. The postsynthetically installed functional groups can be modified through versatile organic chemistry transformations, including (mechanochemical) Suzuki-Miyaura, Sonogashira-Hagihara, and Buchwald-Hartwig amination reactions. Furthermore, the substitutions can be carried out in a sequential manner to yield heterofunctional structures. The edge-functionalization strategy enables modular access to nanostructures with appealing properties, such as strong fluorescence emission in the visible and near-infrared regions (475−900 nm) with record Stokes shifts (>300 nm), at an exceptionally small carbon footprint (C_{48}).

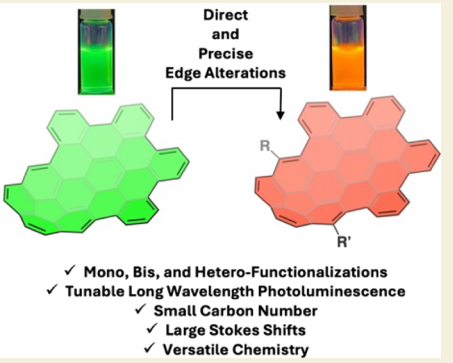

KEYWORDS: *corannulene, coronene, edge-functionalization, electrophilic aromatic substitutions, nanographenes, near-infrared emission, regioselective, stokes shifts*

INTRODUCTION

Electrophilic aromatic substitutions are among the most important reactions in organic chemistry.[1] For decades, these reactions have been essential in providing access to substituted aromatic compounds and enabling studies that facilitate an understanding of the fundamental principles of physical organic chemistry. Small aromatic nuclei represent perfect substrates for such reactions.[1] However, the selectivity of substitution and the reaction scope both become severely limited in the case of polynuclear aromatic hydrocarbons (systems comprising >25 conjugated sp^2-carbon atoms).[2−11] Chlorination remains the most predominant substitution reaction performed directly on pristine nanographenes.[2−11] Due to the absence of selectivity, perchlorination is carried out to avoid the formation of an inseparable product mixture with varying degrees of chlorination.[12,13]

Despite the limitations, direct modification of nanographenes is arguably the most effective approach for introducing substituents into the aromatic scaffold. An alternative approach is to install the substituents on the nanographene precursors.[2−11] This strategy requires the development of separate synthetic routes for differently substituted nanographenes. More importantly, the scope of substituents is often restricted due to their instability or incompatibility under nanographene formation (graphitization) conditions. For instance, intramolecular oxidative cyclodehydrogenation, a prevalent graphitization reaction, could be deterred by steric hindrance or alteration of the electronic energy levels by the substitution.[14−16] A second alternative is *in situ* functionalization of the nanographene scaffold.[17−19] Here, graphitization and functionalization occur simultaneously. However, this approach relies on serendipity and thus remains limited only to chlorination[17] and triflyloxylation.[18,19] In contrast to these approaches, post-synthetic direct substitution on the bare nanographene edge has the advantage of synthetic simplicity, as a single route to the pristine nanographene is required. This pristine aromatic scaffold can then be transformed into targeted structures through substitution reactions. This approach, however, remains underexplored.[12,13,20−28] This limitation is noteworthy as substituents are critical in governing the properties and,

Received: December 15, 2024
Revised: January 31, 2025
Accepted: January 31, 2025
Published: March 24, 2025

Table 1. Examples of Known Highly Emissive Nanographenes[ab]

Entry	Footprint	Nanographene	Φ_f	$^{bs}\lambda_{max}$	$^{em}\lambda_{max}$	Stokes Shift
1	C_{38}	Ovalenes[33−36]	67−89%	580−660 nm	600−670 nm	<10 nm
2	C_{50}	Thia-helicenes[37]	48%	400 nm	666 nm	266 nm
3	C_{68}	Pyrene-helicenes I[38]	93%	538 nm	562 nm	24 nm
4	C_{76}	Pyrene-helicenes II[39]	68%	592 nm	612 nm	20 nm
5	C_{80}	Warped nanographenes[24]	37%	433 nm	528 nm	95 nm
6	C_{102}	Aza-helicenes I[40]	32%	580 nm	588 nm	8 nm
7	C_{124}	Aza-helicenes II[41]	28%	633 nm	770 nm	137 nm
8	C_{138}	Extended helicenes I[42]	18%	510 nm	810 nm	300 nm
9	C_{144}	Thia-helicenes II[43]	14%	630 nm	778 nm	148 nm
10	C_{186}	Extended helicenes II[44]	34%	573 nm	733 nm	160 nm
11	C_{48}	Corannulene−coronenes (this work)	1−82%	350−430 nm	510−695 nm	139−345 nm

[a]The carbon number (number of annulated sp^2-carbon atoms) is shown as footprint. [b]This number represents the fundamental carbon scaffold without consideration for edge substituents.

Scheme 1. (a) Direct Transformation of Corannulene−Coronene Hybrid into Substituted Structures through Selective Electrophilic Aromatic Substitution Reactions on the Nanographene Edge. (b) (i) Bromination: NBS, $BF_3{\cdot}Et_2O$, DCM, rt, 20 min; (ii) Nitration: HNO_3, Ac_2O, rt, 4 h; (iii) Formylation: Cl_2CHOCH_3, $TiCl_4$, DCM, rt, 5 h; (iv) Acylation: CH_3COCl, $AlCl_3$, rt, 24 h

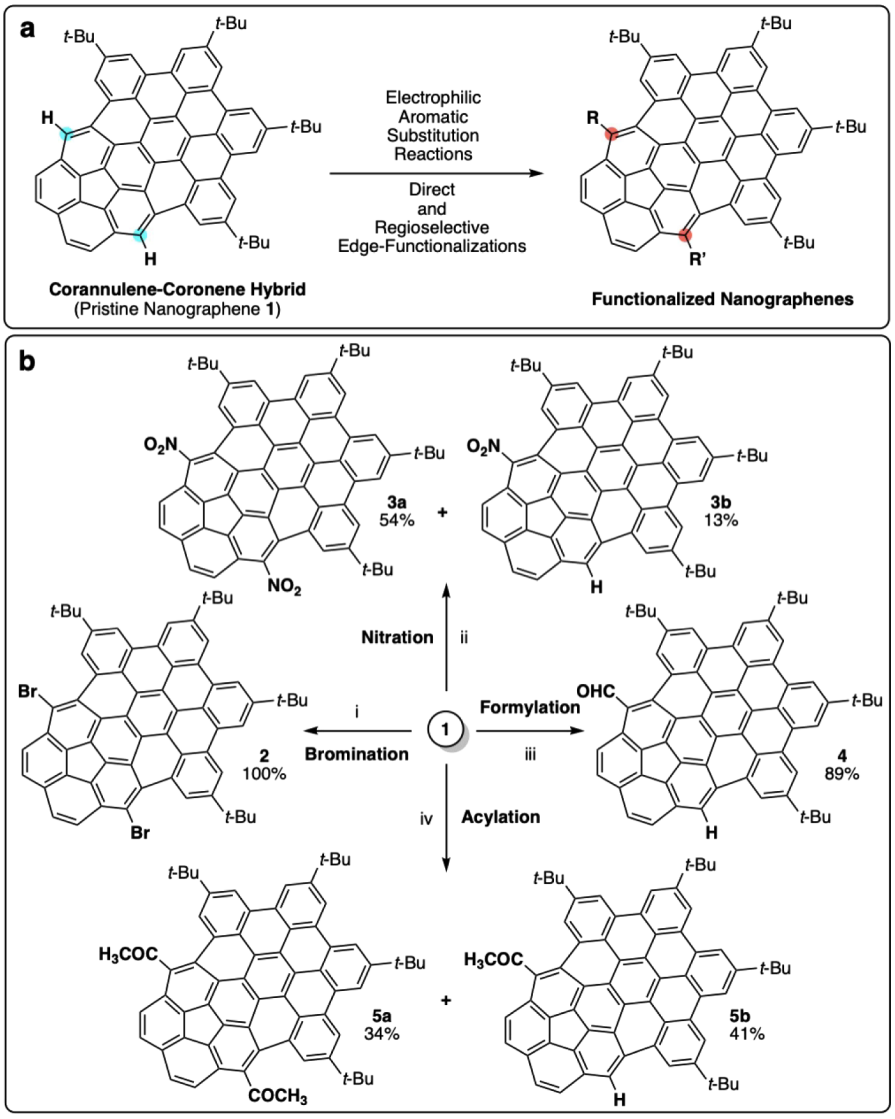

hence, applications of nanographenes. For instance, biological applications necessitate peripheral decoration with hydrophilic chains endowing water solubility to the carbon nanostructures.[24] The alkyl chains, on the other hand, dictate the self-

https://doi.org/10.1021/jacsau.4c01218
JACS Au 2025, 5, 1707−1716

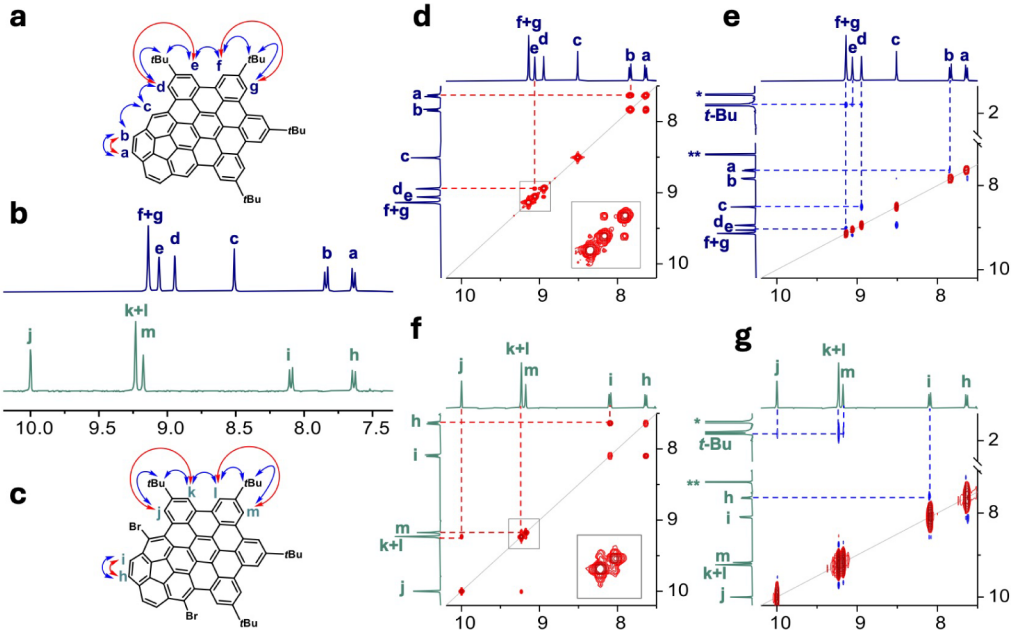

Figure 1. (a) Chemical structure of **1**, showing the COSY and NOESY interactions among different types of protons with the help of red and blue arrows, respectively. (b) Aromatic proton resonances for **1** (top) and **2** (bottom). (c) Chemical structure of **2**, showing the interactions of COSY and NOESY among different types of protons with the help of red and blue arrows, respectively. (d) COSY spectra for **1**. Inset shows the magnified area. (e) NOESY spectra for **1**. (f) COSY spectra for **2**. Inset shows magnified area. (g) NOESY spectra for **2**.

assembly behavior, which ultimately affects their performances in devices.[29] Thus, explorations of direct edge-functionalization routes have become a significant research goal in nanographene chemistry. In this context, we report on a nanographene scaffold that exhibits a considerable scope for electrophilic aromatic substitution reactions. Furthermore, the reactions are regioselective and allow for the practical preparation of a library of edge-functionalized nanographenes beginning with a single pristine substrate. Bifunctional structures can also be obtained through sequential reactions. Multiple substitution patterns lead to a low optical bandgap and strong emissive properties in the visible to the near-infrared range. Typically, such characteristics are achieved by enlarging the aromatic scaffold.[30] However, a loss in solubility and associated challenges in molecular characterization are difficulties encountered in this approach. This is exemplified by the quest to synthesize a soluble C_{222} structure (containing 222 conjugated sp^2-carbon atoms), which was realized only recently.[31,32] Addressing the nanographene edge thus has the advantage that appealing molecular characteristics can be attained at a much lower carbon number (C_{48} in the present case) with the benefits of high solubility and unambiguous structural elucidation.

Besides strong emission in the long-wavelength region to achieve deeper penetration and avoid scattering in biological tissue, another important optical characteristic is represented by the Stokes shift, the difference between the excitation and emission wavelengths. A large difference bodes well for biological imaging applications, as it minimizes crosstalk between the excitation source and observed emission and allows one to generate high-resolution images due to a high signal-to-noise ratio. Although great strides have been made recently in the preparation of emissive nanographene structures (entries 1−10, Table 1),[24,33−44] a strong emission in the deep-red and near-infrared regions along with a large Stokes shift remains rare. Only the members of the helicene family, known to interact with light strongly,[45−49] can achieve this with large systems comprising 124−186 annulated sp^2-carbon atoms (entries 7−10, Table 1).[41−44] On the other hand, commercially available fluorescent dyes with red and near-infrared emission, such as the rhodamine, boron dipyrromethene, and cyanine families, generally exhibit Stokes shifts below 30 nm, while state-of-the-art polycyclic aromatic hydrocarbons optimized for bioimaging purposes boast Stokes shifts in the range of 111−262 nm.[50] In the present work (entry 11, Table 1), accessing long-wavelength emission with record-high Stokes shifts is achieved at an exceptionally small size. The chemistry is also modular, indicating adaptability of molecular structure to meet the requirements of a targeted application. Overall, therefore, this work demonstrates a broad scope for direct regioselective substitutions on the nanographene edge, opportunities for heterofunctionalizations, and the capacity to achieve attractive optoelectronic properties at a small carbon footprint.

RESULTS AND DISCUSSION

Recently, we observed that a corannulene−coronene hybrid structure was chlorinated selectively (R = Cl, Scheme 1a) during an $FeCl_3$-mediated Scholl reaction.[17] A Density Functional Theory (DFT) calculation indicated that the positions adjacent to the newly formed bonds between the planar and the nonplanar segments exhibited the highest Fukui function (f_k^-) values.[17] These positions, therefore, were anticipated to be the most receptive toward further reaction. This prompted us to examine the scope of electrophilic aromatic substitution reactions on the pristine nanographene structure **1** (Scheme 1b).[17] For this, initially, bromination with the help of *N*-bromosuccinimide (NBS) as the brominating agent and boron trifluoride diethyl etherate ($BF_3{\cdot}OEt_2$) as the source of Lewis acid was pursued. The reaction was carried out at room temperature and within minutes led to quantitative conversion to the bis-brominated product **2**. 2D NMR using

https://doi.org/10.1021/jacsau.4c01218
JACS Au 2025, 5, 1707−1716

Scheme 2. Functional Group Transformations[a]

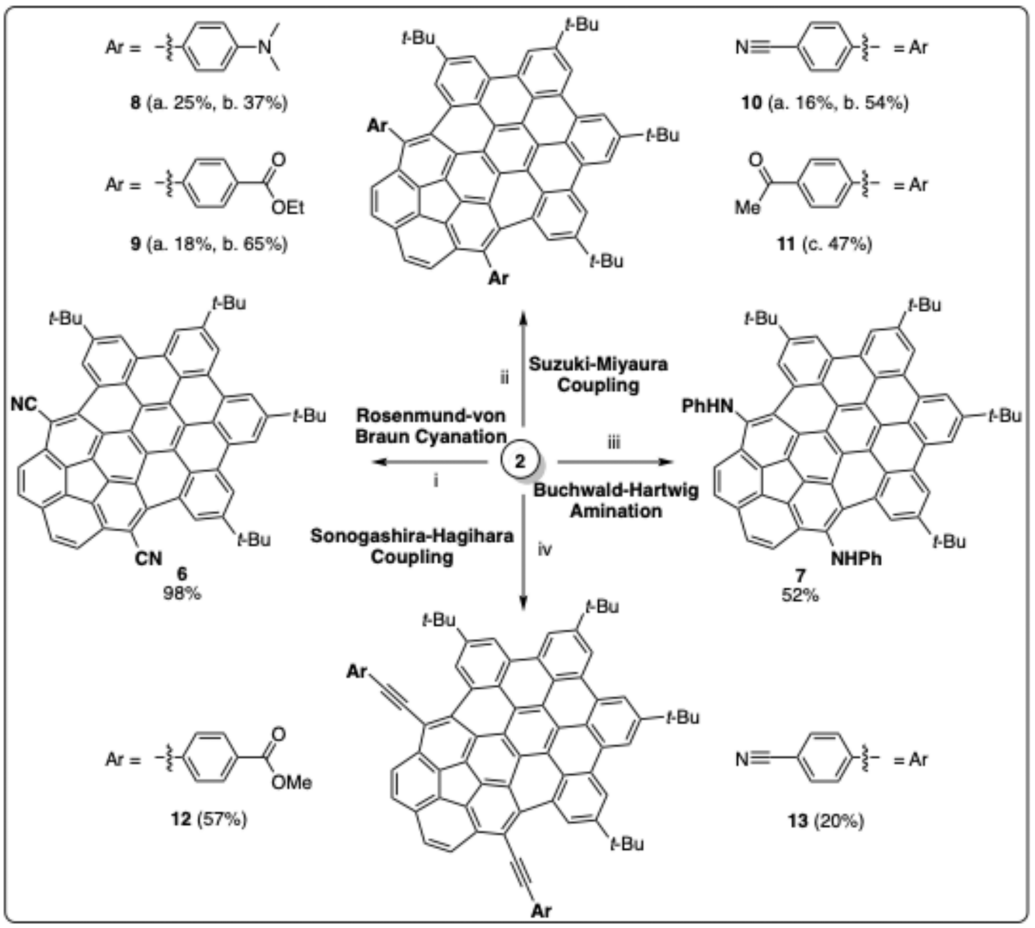

[a](i) Rosenmund-von Braun reaction: CuCN, NMP, 210 °C, 2 h; (ii) Suzuki−Miyaura reaction: a) $PhB(OH)_2$, $Pd(P(t\text{-}Bu)_3)_2$, CsF, dioxane, 80 °C, 72 h; b) Ball milling, 30 Hz, $Pd(OAc)_2$, K_2CO_3, NaCl, 110 °C, 3 h; c) Ball milling, 30 Hz, $Pd(OAc)_2$, K_2CO_3, PPh_3, 125 °C, 1.5 h; (iii) Buchwald−Hartwig reaction: $PhNH_2$, $Pd(dppf)_2Cl_2{\cdot}CH_2Cl_2$, DPPF, NaO*t*-Bu, 130 °C, 72 h; (iv) Sonogashira−Hagihara reaction: $Pd(PPh_3)_2Cl_2$, CuI, NEt_3, THF, 100 °C, 3 h.

correlation spectroscopy (COSY) and nuclear Overhauser effect spectroscopy (NOESY) confirmed the regioselectivity of the substitution reaction (Figure 1).

Encouraged by the quantitative bromination, nitration using a nitric acid and acetic anhydride mixture was carried out. In 4−5 h of reaction time, bis-nitro and mononitro compounds **3a** and **3b** could be isolated in 54 and 13% isolated yields, respectively. A lowering of the reaction time and nitric acid content could be used to favor the monosubstitution to 31%. The Rieche formylation was carried out using dichloromethyl methyl ether acting as the formyl source and titanium tetrachloride ($TiCl_4$) acting as the catalyst. This reaction led to the formation of aldehyde **4** in an 89% isolated yield. In contrast to bromination and nitration, the formylation stopped at monosubstitution, likely due to the mild nature of the electrophile and/or the deactivating nature of the aldehyde substituent. Finally, Friedel−Crafts acylation using $AlCl_3$ and acetyl chloride at room temperature led to the formation of bis-acetyl **5a** and monoacetyl **5b** in isolated yields of 41 and 34%, respectively.

The direct electrophilic aromatic substitution reactions on **1** provided practical access to substituted nanographenes **2**−**5**. Thus, further functional group transformations were targeted (Scheme 2). For this, initially, bis-brominated compound **2** was chosen. A cyanation with copper(I) cyanide (CuCN) led to an efficient transformation to bis-cyano compound **6**. The introduction of electron-withdrawing cyano functionalities directly on the polyaromatic scaffold is seen as a rewarding task as it has the potential to dramatically enhance the electron acceptor properties of the curved aromatic systems.[51,52] Thus, a clean transformation to **6** (98% isolated yield) was encouraging. The introduction of electron donors, on the other hand, is anticipated to enable a red-shift in the absorption spectrum. To achieve this goal, palladium-catalyzed Buchwald−Hartwig C−N cross-coupling lent itself to the installation of amines directly onto the aromatic scaffold in 52% isolated yield (**7**).[53−55]

X-ray crystallography corroborated the regioselectivity conclusions based on the NMR data (Figure 2). These studies also indicated that bowl depth, defined by the distance between the centroid of the central five-membered ring and the mean plane of the ten carbon atoms of the rim, for nanographenes **8**, **9**, and **11** was approximately 1 Å (as compared to 0.87 Å of parental corannulene). In all cases, the molecules interacted via multiple $\pi-\pi$-stacking interactions through their planar aromatic surfaces.

Having installed the electron-withdrawing and electron-donating substituents directly onto the nanographene edge, a

https://doi.org/10.1021/jacsau.4c01218
JACS Au 2025, 5, 1707−1716

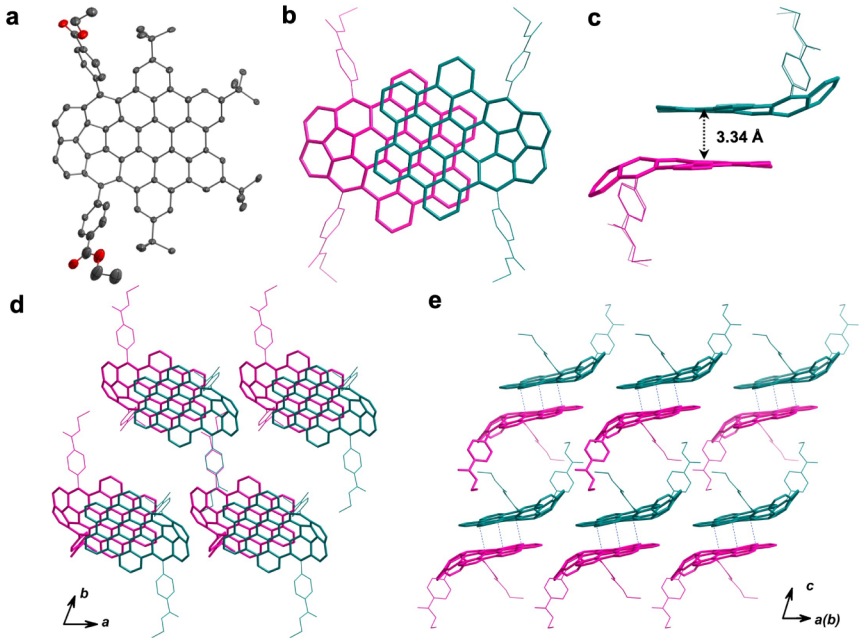

Figure 2. (a,b) Top views of the X-ray crystal structure of **9**, (c) side view, and (d,e) packing structures, along with aromatic stacking interactions between the planar regions of the nanographenes. Thermal ellipsoids were scaled at the 50% probability level. The hydrogen atoms, *t*-Bu groups, and solvent molecules are omitted for clarity.

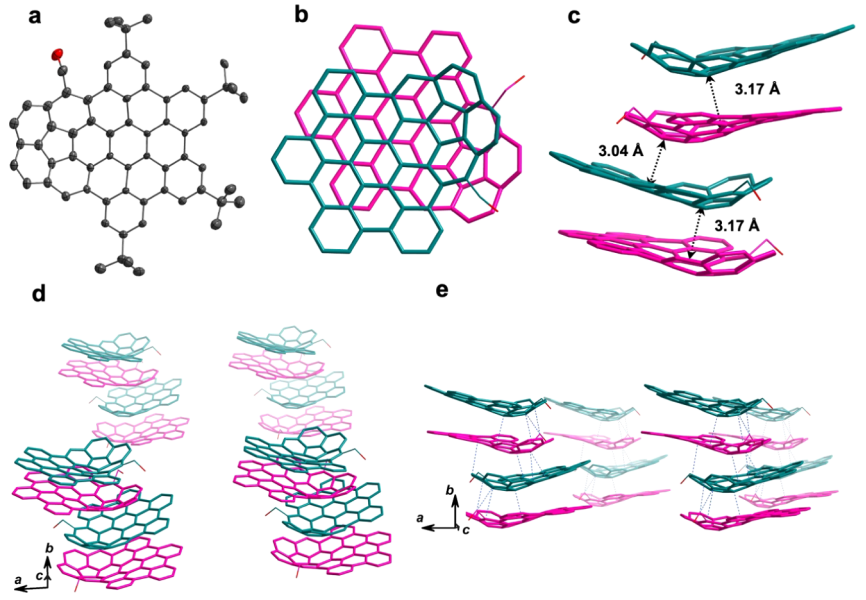

Figure 3. (a,b) Top views of the X-ray crystal structure of **15**, (c) side view, and (d,e) packing structures along with aromatic stacking interactions. Thermal ellipsoids were scaled at the 50% probability level. Hydrogen atoms, *t*-Bu groups, and solvent molecules are omitted for clarity.

linker strategy was considered. For this, a palladium-catalyzed Suzuki−Miyaura reaction was carried out with commercially available boronic acid partners carrying electron-donating dimethylamino and electron-withdrawing cyano and ethyl ester functionalities having a phenyl linker (Scheme 2). These reactions provided targeted compounds **8**−**10** in 16−25% isolated yields. With established protocols for the mechanochemical Suzuki−Miyaura reaction, the product yields could be increased in all cases (37−65%).[56−58] Further benefits of mechanochemistry[59] involved the use of comparatively inexpensive palladium acetate as a catalyst, a much shorter reaction time, and the lack of a need for organic solvent to carry out the reaction.[57] Thus, the next functionalization was carried out only with mechanochemistry and yielded acetyl compound **11** in 47% yield.

The Sonogashira−Hagihara reaction allowed for the installation of phenylene ethynylene groups using commercially available alkynes. Akin to **9** and **10**, **12** and **13** carried cyano and ester groups. These compounds were isolated in 57 and 20% yields, respectively, and demonstrated the corannulene−coronene nanographene substrate to be a feasible partner in multiple metal-catalyzed coupling reactions.

In considering the introduction of electron-donating substituents into the system, an alternative approach would be to reduce the bis-nitro compound **3a** to bis-amines. However, this transformation led to a complex product mixture

https://doi.org/10.1021/jacsau.4c01218
JACS Au 2025, 5, 1707−1716

Scheme 3. (a) Synthesis of Nanographene Amine through Reduction of the Nitro Group; (i) Reduction: $HCOONH_4$, Pd/C, MeOH, 70°C, 3 days. (b) (i) Reduction: $NaBH_4$, THF/MeOH, rt, 5 h; (ii) silylation: TBDMSCl, Imidazole, DCM, rt, 26 h; (iii) nitration: HNO_3, Ac_2O, rt, 24 h; (iv) desilylation: TBAF, THF, rt, 1.5 h

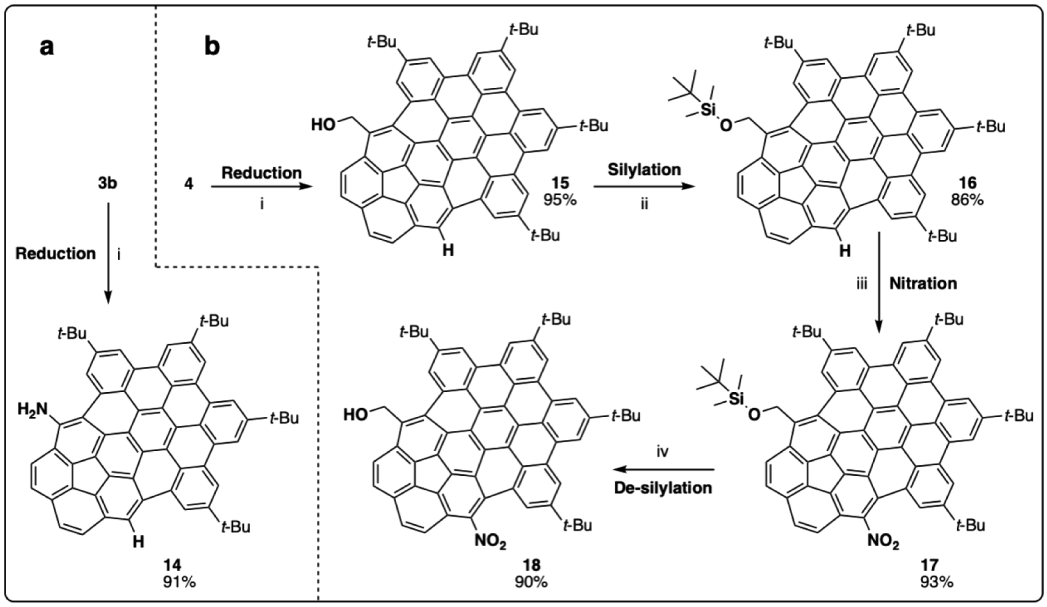

Table 2. Absorbance and Emission Properties of the Nanographenes as Measured in Chloroform at Room Temperature[a]

	Absorbance		Fluorescence		Stokes Shift
Compound	λ_{max} (nm)	$E_{g(opt)}$ (eV)[b]	λ_{em} (nm)[c]	Φ_f (%)[d]	nm[e] (cm^{-1})[f]
Cor[g]	**290**, 320 (sh)[h]	3.57	423, **437**	0.80	147 (8370)
1	**367**, 387, 405 (sh), 457, 490	2.47	**506**, 530 (sh)	21.65	139 (646)
2	347 (sh), **370**, 391, 412, 470, 500	2.35	**650**	0.08	280 (4620)
3a	315, **367**, 405 (sh), 428, 520	2.19	**680**	0.8	313 (4525)
3b	315, **368**, 387 (sh), 409, 470, 505	2.29	**545**, 660	0.73	177 (1450)
4	298, 350 (sh), **368**, 386 (sh), 419, 475, 507	2.28	**570**	11.17	202 (2180)
5a	296, 350 (sh), **368**, 390, 411, 467, 500	2.38	**545**	26.28	177 (1650)
5b	350 (sh), **368**, 387, 408, 460, 495	2.43	**533**	18.22	165 (1440)
6	295, 350 (sh), **370**, 407, 430, 500 (sh), 540	2.13	**598**, 646 (sh)	27.40	228 (1800)
7	**355**, 376, 420, 520	2.19	**588**	20.74	233 (2220)
8	**350**, 421, 496(sh), 550, 613	1.81	**675**	8.34	325 (1500)
9	**350**, 423, 550, 640	1.82	**685**	17.48	335 (1030)
10	335 (sh), **350**, 423, 503, 550, 628	1.78	**695**	9.13	345 (1535)
11	297, 353 (sh), **370**, 391, 413, 466, 496	2.35	**525**, 561 (sh), 685	16.83	155 (1110)
12	300 (sh), 353, **372**, 405, 429, 535	2.13	**573**, 620 (sh)	65.53	201 (1240)
13	300 (sh), 352, **370**, 406, 430, 531	2.11	**579**, 629	82.70	209 (1560)
14	354, **370**, 388, 409, 470, 505	2.29	**555**	13.53	185 (1780)
15	350 (sh), **368**, 386, 412, 460, 490	2.44	**510**, 545 (sh)	18.01	142 (801)
16	340 (sh), **368**, 388, 405, 458, 490	2.45	**510**, 538 (sh)	28.63	142 (801)
17	315, **368**, 388, 412, 470, 505	2.29	**513**, 548 (sh), 665 (sh)	3.03	145 (308)
18	315, **368**, 390, 413, 470, 503	2.29	**660**	0.42	292 (4730)

[a]The wavelength in bold indicates the major signal. [b]Calculated from the long-wavelength absorption edge ($E_{g(opt)} = 1240/\lambda_{onset}$). [c]Obtained by exciting each absorption maximum. [d]Calculated using integration sphere (conc ~6×10^{-6}). [e]Stokes shift in nm is calculated as the difference between absorption and emission maxima.[53] [f]Stokes shift in cm^{-1} is calculated as the difference between lowest energy absorption band and emission maximum. [g]Cor = corannulene. [h]sh = shoulder.

that could not be separated. Thus, mononitro compound **3b** was used instead and led to a successful reduction to monoamine **14** in an isolated yield of 91% (Figure 3a).

The monosubstituted structures offer the opportunity for introducing a second functional group as a reactive site remains available for a further substitution reaction. This avenue was explored with the help of compound **4** (Scheme 3b). The aldehyde group was first reduced with the help of sodium borohydride (**15**) and then masked with the help of the *tert*-butyldimethylsilyl (TBDMS) group (**16**). A nitration to **17** and removal of the protecting group furnished heterofunctional nanographene **18**. These preliminary results suggest that the other monosubstituted structures (mononitro (**3b**), acyl (**5b**), and amine (**14**)) are potential precursors for a heterobifunctionalization strategy to further enhance molecular complexity and function. The X-ray crystal structure of **15**

https://doi.org/10.1021/jacsau.4c01218
JACS Au 2025, 5, 1707−1716

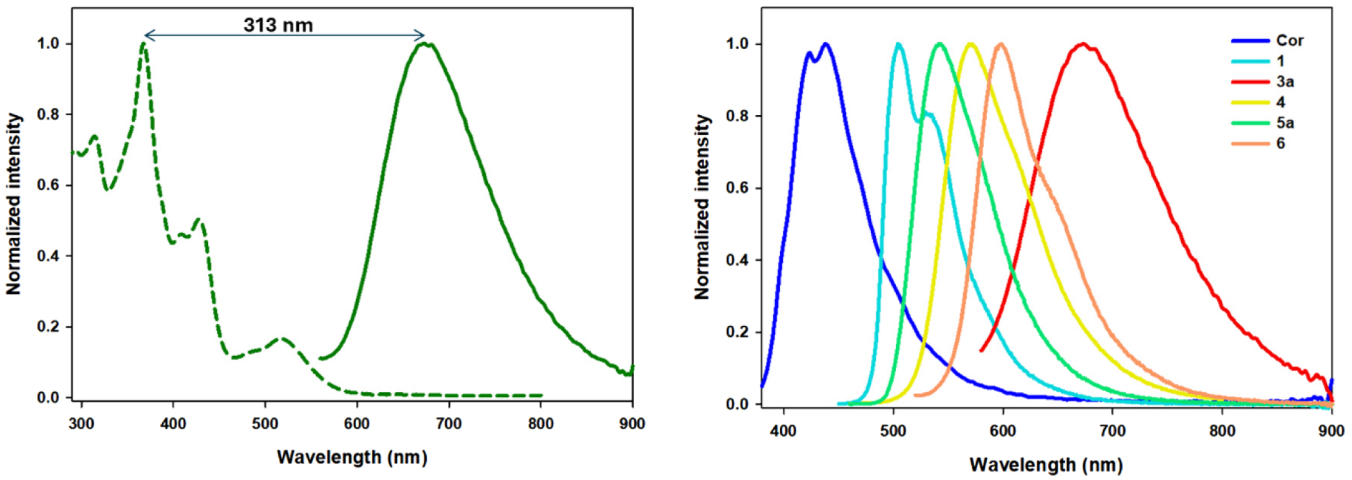

Figure 4. UV−vis absorption and fluorescence emission of **3a** underlining Stokes shifts typical in the present family of nanographenes (left). Emission spectra of some of the nanographenes highlight spectral tunability (right).

confirmed the regioselectivity of monofunctionalization (Figure 3).

The number and nature of the substituents had a significant impact on the optical properties (Table 2 and Figure 4). As anticipated, fluorescence emission was low for molecules carrying halogen atoms or nitro groups.[60,61] Monoaldehyde showed broad emission within the 500−800 nm range with a quantum yield (Φ_f) of 11%. The placement of a ketone group increased Φ_f to 18%. The introduction of a second ketone further increased photoluminescence to 26%. Cyano substituents showed similarly high Φ_f (27%) in the yellow-red region. The placement of phenylamines retained this emission range with a Φ_f of 20%. The phenyl-linked systems exhibited emission in the red to near-infrared region (λ_{edge} = 900 nm) with a good Φ_f of 10−17%. An introduction of planar acetylene π-bridges led to materials with an excellent Φ_f of 65−82%. This observation was akin to the fluorenyl-2,7-ethynylene motif, which can be traced on the nanographene surface and is known to exhibit a quantum yield of unity, albeit in the UV range.[62,63] The advantage of this motif in the nanographene setting thus leads to highly emissive materials in the red region. Finally, the TBDMS-carrying compound exhibited a Φ_f of 28%, the highest among nonacetylene structures.

The versatility of the current emissive nanographene family is similar to ovalenes, which have found great success as fluorescent probes in biology.[33−36] The ovalenes (λ_{edge} = 800 nm) display higher quantum yields, but their Stokes shifts are limited to only a few nanometers. In comparison, the current materials are significantly red-shifted (λ_{edge} = 900 nm) and display the largest Stokes shifts (>300 nm), calculated in accordance with Xie and Finney,[53] known thus far. Typically, Stokes shifts are given in cm^{-1} as the distance between the lowest energy absorption and λ_{max} of emission. However, we have emphasized the difference between λ_{max} of absorption and λ_{max} of emission in nm, as in bioimaging applications the excitation does not have to be at the lowest energy wavelength. To maximize the difference between the excitation and the emission wavelengths, as described in the introduction, sample excitation can be carried out at the λ_{max} of absorption. Overall, thus, the current materials are expected to lead to emissive probes for high-resolution bioimaging applications. To achieve the water solubility necessary for such purposes, a transesterification reaction of **9** with polyethylene glycol monomethyl ether or the use of a polyethylene glycol-based aryl boronic acid as a coupling partner with **2** can be envisaged. This molecular pliability is also a feature that distinguishes the current concept from helicenes,[41−44] which are extraordinary in their structure and function but lack versatility (in terms of structural adaptability), helicenes (entries 7−10, Table 1) belong to the first alternative described in the Introduction).

CONCLUSION

In summary, a corannulene−coronene hybrid structure is shown to be receptive toward multiple electrophilic aromatic substitution reactions at the nanographene edge. The substitutions are direct, selective, and yield good results . Thus, a new family of precisely functionalizable nanostructures can be accessed in a practical manner from a single substrate. The functionalizations can be sequential, thus allowing for the formation of heterofunctional structures. The structures exhibit edge-dependent optical properties that can be modulated through simple functional group transformations. In some cases, the emission extends into the near-infrared region. The results indicate that attractive optoelectronic properties, which are often accessed by enlarging the number of aromatic annulations and encountering typical solubility and characterization problems, can be achieved with a small carbon footprint, offering the advantages of high solubility and unambiguous characterization through molecular engineering at the nanographene edge. Since the chemistry is modular, edge functionalization with electron-rich and -deficient heterocycles carrying nitrogen, chalcogens, silicon, and boron can be envisaged to further gain a change in absorption and emission range and quantum yields. The ability to heterofunctionalize could lead to the placement of donor/acceptor substituents at the nanographene edge. The placement of cationic groups at the aryl substituents could potentially bring specific cellular uptake properties, such as the mitochondria-targeting capacity of phosphonium or the antibacterial capacity of ammonium and sulfonium salts. In these cases, the inherent optoelectronic properties can be used to image and track the location of the nanographene, as well as potentially generate reactive oxygen species[24,31,64] for therapeutic purposes, thus leading to a new family of nanographene-based theragnostic materials.

https://doi.org/10.1021/jacsau.4c01218
JACS Au 2025, 5, 1707−1716

METHODS

The pristine nanographene was obtained through palladium-catalyzed dichlorination in an inert atmosphere in tetrahydrofuran in the presence of potassium carbonate and triphenylphosphine at 80 °C for a period of 5 h. The reaction mixture was filtered through a short pad of silica gel and washed with dichloromethane. The filtrate was concentrated under reduced pressure, and the crude residue was purified by flash chromatography using hexane and dichloromethane (9:1) as the eluent to furnish **1** in 99% isolated yield as an orange−yellow solid. This material was then used for further nanographene modification studies.

ASSOCIATED CONTENT

Data Availability Statement

The data that support the findings of this study are available in the Supporting Information of this article.

Supporting Information

The Supporting Information is available free of charge at https://pubs.acs.org/doi/10.1021/jacsau.4c01218.

Details on experimental procedures, characterization data, mass spectra, NMR spectra, X-ray crystallography data, and optical spectra of all the compounds(PDF)
Crystal data of 8(PDF)
Crystal data of 9(PDF)
Crystal data of 11(PDF)
Crystal data of 15 (PDF)

AUTHOR INFORMATION

Corresponding Author

Mihaiela C. Stuparu − *School of Chemistry, Chemical Engineering and Biotechnology, Nanyang Technological University, Singapore 637371, Singapore; National Institute for Research and Development of Isotopic and Molecular Technologies - INCDTIM, Cluj-Napoca 400293, Romania;* orcid.org/0000-0001-8663-6189; Email: mstuparu@ntu.edu.sg

Authors

Jovana Stanojkovic − *School of Chemistry, Chemical Engineering and Biotechnology, Nanyang Technological University, Singapore 637371, Singapore*

Natalia Terenti − *National Institute for Research and Development of Isotopic and Molecular Technologies - INCDTIM, Cluj-Napoca 400293, Romania*

Complete contact information is available at: https://pubs.acs.org/10.1021/jacsau.4c01218

Author Contributions

The manuscript was written through contributions of all authors. All authors have given approval to the final version of the manuscript.

Notes

The authors declare no competing financial interest.

ACKNOWLEDGMENTS

This work was financially supported by the Ministry of Education, Singapore, under the AcRF Tier 2 (MOE-T2EP10221-0002) and by the Ministry of Research, Innovation and Digitalization under Romania's National Recovery and Resilience Plan PNRR−III-C9-2022−I8 program with Project code 167/15.11.22.

REFERENCES

(1) *March's Advanced Organic Chemistry: Reactions, Mechanisms, and Structure*, 6th ed., Smith, M. B.; March, J., Eds.; Wiley Interscience: New York, 2006.
(2) Gu, Y.; Qiu, Z.; Müllen, K. Nanographenes and Graphene Nanoribbons as Multitalents of Present and Future Materials Science. *J. Am. Chem. Soc.* **2022**, *144* (26), 11499−11524.
(3) Narita, A.; Wang, X. Y.; Feng, X.; Müllen, K. New advances in nanographene chemistry. *Chem. Soc. Rev.* **2015**, *44* (18), 6616−6643.
(4) Tsefrikas, V. M.; Scott, L. T. Geodesic polyarenes by flash vacuum pyrolysis. *Chem. Rev.* **2006**, *106* (12), 4868−4884.
(5) Liu, J.; Feng, X. Synthetic Tailoring of Graphene Nanostructures with Zigzag-Edged Topologies: Progress and Perspectives. *Angew. Chem., Int. Ed.* **2020**, *59* (52), 23386−23401.
(6) Wang, X.-Y.; Yao, X.; Narita, A.; Müllen, K. Heteroatom-Doped Nanographenes with Structural Precision. *Acc. Chem. Res.* **2019**, *52* (9), 2491−2505.
(7) Stępień, M.; Gońka, E.; Żyła, M.; Sprutta, N. Heterocyclic Nanographenes and Other Polycyclic Heteroaromatic Compounds: Synthetic Routes, Properties, and Applications. *Chem. Rev.* **2017**, *117* (4), 3479−3716.
(8) Majewski, M. A.; Stępień, M. Bowls, Hoops, and Saddles: Synthetic Approaches to Curved Aromatic Molecules. *Angew. Chem., Int. Ed.* **2019**, *58* (1), 86−116.
(9) Pun, S. H.; Miao, Q. Toward Negatively Curved Carbons. *Acc. Chem. Res.* **2018**, *51* (7), 1630−1642.
(10) Pozo, I.; Guitian, E.; Perez, D.; Pena, D. Synthesis of Nanographenes, Starphenes, and Sterically Congested Polyarenes by Aryne Cyclotrimerization. *Acc. Chem. Res.* **2019**, *52* (9), 2472−2481.
(11) Zhu, Y.; Wang, J. Helical Synthetic Nanographenes with Atomic Precision. *Acc. Chem. Res.* **2023**, *56* (3), 363−373.
(12) Tan, Y. Z.; Yang, B.; Parvez, K.; Narita, A.; Osella, S.; Beljonne, D.; Feng, X.; Müllen, K. Atomically precise edge chlorination of nanographenes and its application in graphene nanoribbons. *Nat. Commun.* **2013**, *4*, 2646.
(13) Liu, Y.-M.; Hou, H.; Zhou, Y.-Z.; Zhao, X.-J.; Tang, C.; Tan, Y.-Z.; Müllen, K. Nanographenes as electron-deficient cores of donor-acceptor systems. *Nat. Commun.* **2018**, *9* (1), 1901.
(14) Grzybowski, M.; Sadowski, B.; Butenschon, H.; Gryko, D. T. Synthetic Applications of Oxidative Aromatic Coupling-From Biphenols to Nanographenes. *Angew. Chem., Int. Ed.* **2020**, *59* (8), 2998−3027.
(15) Grzybowski, M.; Skonieczny, K.; Butenschön, H.; Gryko, D. T. Comparison of Oxidative Aromatic Coupling and the Scholl Reaction. *Angew. Chem., Int. Ed.* **2013**, *52* (38), 9900−9930.
(16) Zhang, Y.; Pun, S. H.; Miao, Q. The Scholl Reaction as a Powerful Tool for Synthesis of Curved Polycyclic Aromatics. *Chem. Rev.* **2022**, *122* (18), 14554−14593.
(17) Stanojkovic, J.; William, R.; Zhang, Z.; Fernandez, I.; Zhou, J.; Webster, R. D.; Stuparu, M. C. Synthesis of precisely functionalizable curved nanographenes via graphitization-induced regioselective chlorination in a mechanochemical Scholl Reaction. *Nat. Commun.* **2023**, *14* (1), 803.
(18) Yang, X.; Hoffmann, M.; Rominger, F.; Kirschbaum, T.; Dreuw, A.; Mastalerz, M. Functionalized Contorted Polycyclic Aromatic Hydrocarbons by a One-Step Cyclopentannulation and Regioselective Triflyloxylation. *Angew. Chem., Int. Ed.* **2019**, *58* (31), 10650−10654.
(19) Yang, X.; Rominger, F.; Mastalerz, M. Contorted Polycyclic Aromatic Hydrocarbons with Two Embedded Azulene Units. *Angew. Chem., Int. Ed.* **2019**, *58* (49), 17577−17582.
(20) Holzwarth, J.; Amsharov, K. Y.; Sharapa, D. I.; Reger, D.; Roshchyna, K.; Lungerich, D.; Jux, N.; Hauke, F.; Clark, T.; Hirsch, A. Highly Regioselective Alkylation of Hexabenzocoronenes: Fundamental Insights into the Covalent Chemistry of Graphene. *Angew. Chem., Int. Ed.* **2017**, *56* (40), 12184−12190.

(21) Ruan, L.; Luo, W.; Zhang, H.; Liu, P.; Shi, Y.; An, P. Cycl[2,2,4]azine-embedded non-alternant nanographenes containing fused antiaromatic azepine ring. *Chem. Sci.* **2024**, *15* (4), 1511−1519.
(22) Eliseeva, M. N.; Scott, L. T. Pushing the Ir-catalyzed C-H polyborylation of aromatic compounds to maximum capacity by exploiting reversibility. *J. Am. Chem. Soc.* **2012**, *134* (37), 15169−15172.
(23) Kato, K.; Lin, H. A.; Kuwayama, M.; Nagase, M.; Segawa, Y.; Scott, L. T.; Itami, K. Two-step synthesis of a red-emissive warped nanographene derivative via a ten-fold C-H borylation. *Chem. Sci.* **2019**, *10* (39), 9038−9041.
(24) Lin, H. A.; Sato, Y.; Segawa, Y.; Nishihara, T.; Sugimoto, N.; Scott, L. T.; Higashiyama, T.; Itami, K. A Water-Soluble Warped Nanographene: Synthesis and Applications for Photoinduced Cell Death. *Angew. Chem., Int. Ed.* **2018**, *57* (11), 2874−2878.
(25) Chen, Q.; Wang, D.; Baumgarten, M.; Schollmeyer, D.; Müllen, K.; Narita, A. Regioselective Bromination and Functionalization of Dibenzo[hi,st]ovalene as Highly Luminescent Nanographene with Zigzag Edges. *Chem.-Asian J.* **2019**, *14* (10), 1703−1707.
(26) Li, G.; Phan, H.; Herng, T. S.; Gopalakrishna, T. Y.; Liu, C.; Zeng, W.; Ding, J.; Wu, J. Toward Stable Superbenzoquinone Diradicaloids. *Angew. Chem., Int. Ed.* **2017**, *56* (18), 5012−5016.
(27) Zhang, Q.; Kawasumi, K.; Segawa, Y.; Itami, K.; Scott, L. T. Palladium-Catalyzed C−H Activation Taken to the Limit. Flattening an Aromatic Bowl by Total Arylation. *J. Am. Chem. Soc.* **2012**, *134* (38), 15664−15667.
(28) Kawasumi, K.; Zhang, Q.; Segawa, Y.; Scott, L. T.; Itami, K. A grossly warped nanographene and the consequences of multiple odd-membered-ring defects. *Nat. Chem.* **2013**, *5*, 739−744.
(29) Wu, J.; Watson, M. D.; Müllen, K. The versatile synthesis and self-assembly of star-type hexabenzocoronenes. *Angew. Chem., Int. Ed.* **2003**, *42* (43), 5329−5333.
(30) Rieger, R.; Müllen, K. Forever young: polycyclic aromatic hydrocarbons as model cases for structural and optical studies. *J. Phys. Org. Chem.* **2010**, *23* (4), 315−325.
(31) Ma, X. H.; Gao, X.; Chen, J. Y.; Cao, M.; Dai, Q.; Jia, Z. K.; Zhou, Y. B.; Zhao, X. J.; Chu, C.; Liu, G. Soluble Nanographene C(222): Synthesis and Applications for Synergistic Photodynamic/Photothermal Therapy. *J. Am. Chem. Soc.* **2024**, *146* (4), 2411−2418.
(32) Zhang, Z.; Zhu, H.; Gu, J.; Shi, H.; Hirose, T.; Jiang, L.; Zhu, Y.; Zhong, D.; Wang, J. Nonplanar Nanographene with a Large Conjugated pi-Surface. *J. Am. Chem. Soc.* **2024**, *146* (35), 24681−24688.
(33) Chen, Q.; Thoms, S.; Stottinger, S.; Schollmeyer, D.; Müllen, K.; Narita, A.; Basche, T. Dibenzo[hi,st]ovalene as Highly Luminescent Nanographene: Efficient Synthesis via Photochemical Cyclodehydroiodination, Optoelectronic Properties, and Single-Molecule Spectroscopy. *J. Am. Chem. Soc.* **2019**, *141* (41), 16439−16449.
(34) Liu, X.; Chen, S. Y.; Chen, Q.; Yao, X.; Gelleri, M.; Ritz, S.; Kumar, S.; Cremer, C.; Landfester, K.; Müllen, K. Nanographenes: Ultrastable, Switchable, and Bright Probes for Super-Resolution Microscopy. *Angew. Chem., Int. Ed.* **2020**, *59* (1), 496−502.
(35) Jin, E.; Yang, Q.; Ju, C. W.; Chen, Q.; Landfester, K.; Bonn, M.; Müllen, K.; Liu, X.; Narita, A. A Highly Luminescent Nitrogen-Doped Nanographene as an Acid- and Metal-Sensitive Fluorophore for Optical Imaging. *J. Am. Chem. Soc.* **2021**, *143* (27), 10403−10412.
(36) Zhu, X.; Chen, Q.; Zhao, H.; Yang, Q.; Goudappagouda; Gelleri, M.; Ritz, S.; Ng, D.; Koynov, K.; Parekh, S. H. Intrinsic Burst-Blinking Nanographenes for Super-Resolution Bioimaging. *J. Am. Chem. Soc.* **2024**, *146* (8), 5195−5203.
(37) Yang, W.-W.; Ren, Z.-H.; Feng, J.; Lv, Z. B.; Cheng, X.; Zhang, J.; Du, D.; Chi, C.; Shen, J. J. A Deep-Red Emissive Sulfur-Doped Double [7]Helicene Photosensitizer: Synthesis, Structure and Chiral Optical Properties. *Angew. Chem., Int. Ed.* **2024**, *63* (45), No. e202412681.
(38) Li, J.-K.; Chen, X.-Y.; Zhao, W. L.; Guo, Y. L.; Zhang, Y.; Wang, X. C.; Sue, A. C.; Cao, X. Y.; Li, M.; Chen, C. F.; Wang, X.-Y. Synthesis of Highly Luminescent Chiral Nanographene. *Angew. Chem., Int. Ed.* **2023**, *62* (4), No. e202215367.
(39) Dong, Y.; Zhang, Z.; Hashikawa, Y.; Meng, H.; Bai, F.; Itami, K.; Chaolumen. Chaolumen. A Double Twisted Nanographene with a Contorted Pyrene Core. *Angew. Chem., Int. Ed.* **2024**, *63* (35), No. e202406927.
(40) Qiu, S.; Valdivia, A. C.; Zhuang, W.; Hung, F. F.; Che, C. M.; Casado, J.; Liu, J. Nonalternant Nanographenes Containing N-Centered Cyclopenta[ef]heptalene and Aza[7]Helicene Units. *J. Am. Chem. Soc.* **2024**, *146* (23), 16161−16172.
(41) Wu, Y. F.; Ying, S. W.; Su, L. Y.; Du, J. J.; Zhang, L.; Chen, B. W.; Tian, H. R.; Xu, H.; Zhang, M. L.; Yan, X. Nitrogen-Embedded Quintuple [7]Helicene: A Helicene-Azacorannulene Hybrid with Strong Near-Infrared Fluorescence. *J. Am. Chem. Soc.* **2022**, *144* (24), 10736−10742.
(42) Tan, J.; Xu, X.; Liu, J.; Vasylevskyi, S.; Lin, Z.; Kabe, R.; Zou, Y.; Müllen, K.; Narita, A.; Hu, Y. Synthesis of a π-Extended Double [9]Helicene. *Angew. Chem., Int. Ed.* **2023**, *62* (18), No. e202218494.
(43) Wu, Y. F.; Ying, S. W.; Liao, S. D.; Zhang, L.; Du, J. J.; Chen, B. W.; Tian, H. R.; Xie, F. F.; Xu, H.; Deng, S. L.; Zhang, Q. Sulfur-Doped Quintuple [9]Helicene with Azacorannulene as Core. *Angew. Chem., Int. Ed. Engl.* **2022**, *61* (33), No. e202204334.
(44) Chen, Y.; Lin, C.; Luo, Z.; Yin, Z.; Shi, H.; Zhu, Y.; Wang, J. Double pi-Extended Undecabenzo[7]helicene. *Angew. Chem., Int. Ed.* **2021**, *60* (14), 7796−7801.
(45) Wang, Y.; Yin, Z.; Zhu, Y.; Gu, J.; Li, Y.; Wang, J. Hexapole [9]Helicene. *Angew. Chem., Int. Ed.* **2019**, *58* (2), 587−591.
(46) Pun, S. H.; Cheung, K. M.; Yang, D.; Chen, H.; Wang, Y.; Kershaw, S. V.; Miao, Q. A Near-Infrared Absorbing and Emissive Quadruple Helicene Enabled by the Scholl Reaction of Perylene. *Angew. Chem., Int. Ed.* **2022**, *61* (8), No. e202113203.
(47) Zhu, Y.; Guo, X.; Li, Y.; Wang, J. Fusing of Seven HBCs toward a Green Nanographene Propeller. *J. Am. Chem. Soc.* **2019**, *141* (13), 5511−5517.
(48) Guo, X.; Yuan, Z.; Zhu, Y.; Li, Z.; Huang, R.; Xia, Z.; Zhang, W.; Li, Y.; Wang, J. A Nitrogen-Doped Hexapole [7]Helicene versus Its All-Carbon Analogue. *Angew. Chem., Int. Ed.* **2019**, *58* (47), 16966−16972.
(49) Zhang, Z.; Csókás, D.; Fernández, I.; Stuparu, M. C. Chiral stacks of a curved nanographene. *Chem* **2024**, *10* (10), 3199−3211.
(50) Yang, J.; Xu, Z.; Yu, L.; Wang, B.; Hu, R.; Tang, J.; Lv, J.; Xiao, H.; Tan, X.; Wang, G.; Li, J.-X. Organic Fluorophores with Large Stokes Shift for the Visualization of Rapid Protein and Nucleic Acid Assays. *Angew. Chem., Int. Ed.* **2024**, *63* (17), No. e202318800.
(51) Haupt, A.; Lentz, D. Corannulenes with Electron-Withdrawing Substituents: Synthetic Approaches and Resulting Structural and Electronic Properties. *Chem. -Eur. J.* **2019**, *25* (14), 3440−3454.
(52) Haupt, A.; Walter, R.; Loll, B.; Lentz, D. Tetracyanocorannulene − an Easily Accessible and Strongly Electron-Deficient Compound. *Eur. J. Org. Chem.* **2018**, *2018* (45), 6338−6342.
(53) Xie, F.; Finney, N. S. Synthesis and optical properties of mono- and diaminocorannulenes. *Chem. Commun.* **2020**, *56* (72), 10525−10528.
(54) Ghosh, A.; Csokas, D.; Budanovic, M.; Webster, R. D.; Papai, I.; Stuparu, M. C. Synthesis of azahelicenes through Mallory reaction of imine precursors: corannulene substrates provide an exception to the rule in oxidative photocyclizations of diarylethenes. *Chem. Sci.* **2021**, *12* (11), 3977−3983.
(55) Huang, L.; Wang, Q.; Fu, P.; Sun, Y.; Xu, J.; Browne, D. L.; Huang, J. Extended Quinolizinium-Fused Corannulene Derivatives: Synthesis and Properties. *JACS Au* **2024**, *4* (4), 1623−1631.
(56) Bati, G.; Csokas, D.; Yong, T.; Tam, S. M.; Shi, R. R. S.; Webster, R. D.; Papai, I.; Garcia, F.; Stuparu, M. C. Mechanochemical Synthesis of Corannulene-Based Curved Nanographenes. *Angew. Chem., Int. Ed.* **2020**, *59* (48), 21620−21626.
(57) Seo, T.; Kubota, K.; Ito, H. Mechanochemistry-Directed Ligand Design: Development of a High-Performance Phosphine Ligand for Palladium-Catalyzed Mechanochemical Organoboron Cross-Coupling. *J. Am. Chem. Soc.* **2023**, *145* (12), 6823−6837.

https://doi.org/10.1021/jacsau.4c01218
JACS Au 2025, 5, 1707−1716

(58) Seo, T.; Toyoshima, N.; Kubota, K.; Ito, H. Tackling Solubility Issues in Organic Synthesis: Solid-State Cross-Coupling of Insoluble Aryl Halides. *J. Am. Chem. Soc.* **2021**, *143* (16), 6165−6175.
(59) Cuccu, F.; De Luca, L.; Delogu, F.; Colacino, E.; Solin, N.; Mocci, R.; Porcheddu, A. Mechanochemistry: New Tools to Navigate the Uncharted Territory of "Impossible" Reactions. *ChemSuschem* **2022**, *15* (17), No. e202200362.
(60) Turro, N. J. *Modern molecular photochemistry*; University Science Books, 1991.
(61) For exceptional cases in nitroaromatics, see Poronik, Y. M.; Sadowski, B.; Szychta, K.; Quina, F. H.; Vullev, V. I.; Gryko, D. T. Revisiting the non-fluorescence of nitroaromatics: presumption versus reality. *J. Mater. Chem. C* **2022**, *10* (8), 2870−2904.
(62) Birckner, E.; Grummt, U.-W.; Goller, A. H.; Pautzsch, T.; Egbe, D. A. M.; Al-Higari, M.; Klemm, E. Photophysics of Arylene and Heteroaryleneethinylenes. *J. Phys. Chem. A* **2001**, *105* (45), 10307−10315.
(63) Ethynyl-substitution of corannulene bowl is also known to enhance quantum yield of emission Wu, Y.-T.; Bandera, D.; Maag, R.; Linden, A.; Baldridge, K. K.; Siegel, J. S. Multiethynyl Corannulenes: Synthesis, Structure, and Properties. *J. Am. Chem. Soc.* **2008**, *130* (32), 10729−10739.
(64) Ju, Y.-Y.; Shi, X. X.; Xu, S. Y.; Ma, X. H.; Wei, R. J.; Hou, H.; Chu, C. C.; Sun, D.; Liu, G.; Tan, Y. Z. Atomically Precise Water-Soluble Graphene Quantum Dot for Cancer Sonodynamic Therapy. *Adv. Sci.* **2022**, *9* (19), 2105034.

https://doi.org/10.1021/jacsau.4c01218
JACS Au 2025, 5, 1707−1716